LANGMUIR Article
Cite This: Langmuir 2018, 34, 5935−5942
pubs.acs.org/Langmuir

Allosteric Self-Assembly of Coordinating Terthiophene Amphiphile for Triggered Light Harvesting

Tian Huang,[†,‡] Zhiyang Zhu,[†] Rongrong Xue,[†] Tongyue Wu,[†] Peilong Liao,[†] Zeyu Liu,[†] Yunlong Xiao,*[,†] Jianbin Huang,[†] and Yun Yan*[,†]

[†]Beijing National Laboratory for Molecular Sciences (BNLMS), State Key Laboratory for Structural Chemistry of Unstable and Stable Species, College of Chemistry and Molecular Engineering, and [‡]Academy for Advanced Interdisciplinary Studies, Peking University, Beijing 100871, China

Supporting Information

ABSTRACT: Allosteric regulation is extensively employed by nature to achieve functional control of protein or deoxyribonucleic acid through triggered conformational change at a remote site. We report that a similar strategy can be utilized in artificial self-assembly to control the self-assembled structure and its function. We show that on binding of metal ions to the headgroup of an amphiphile TTC4L, the conformational change may lead to change of the dipole orientation of the energy donor at the chain end. This on the one hand leads to a drastically different self-assembled structure; on the other hand, it enables light harvesting between the donor−acceptor. Because the Forster resonance fluorescence transfer efficiency is gated by metal ions, controlling the feeding of metal ions allows switching on and off of light harvesting. We expect that using allosteric self-assembly, we will be able to create abundant structures with distinct function from limited molecules, which show prominent potential for the postorganic modification of the structure and function of self-assembled materials.

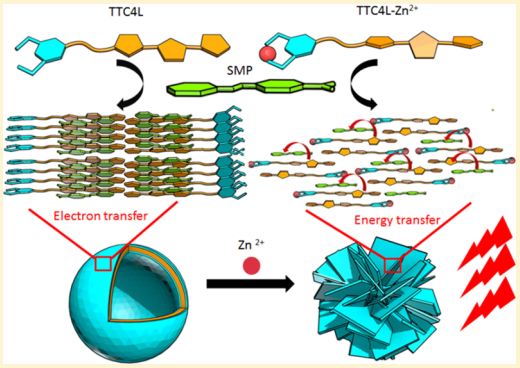

INTRODUCTION

One of the marvellous magic of nature is to employ allosteric effect,[1−4] namely, to regulate the function of protein[5−7] or deoxyribonucleic acid (DNA)[8−10] through conformational or dynamic changes. Typical allosteric effect refers to binding a molecule at one site but changing the binding ability at a remote site.[11−13] Using this strategy, various complex and precise functions are created by nature with limited compositions. Similarly, allosteric regulation is also employed by chemists to achieve the desired sensor or detection effect.[14,15] However, so far, examples for artificial allosteric regulation are limited on the molecular level,[16,17] where the distance or interaction between two groups within one molecule is controlled by triggered conformational variation of the molecule. This is in clear contrast to the complexity in natural allostery, where the stimuli act at one end, but functional changes occur at a remote end. Furthermore, many self-assembled structures, such as β-sheets or α-helices in protein and base-pairs in DNA, participate in the transduction of signals triggered by a remote stimulus. In analogy to allostery in nature, we expect that functional control over the artificial systems can be achieved by allosteric effect that occurs in molecular self-assembly.

Among various functional materials, light-harvesting systems based on the Forster resonance fluorescence transfer (FRET) have attracted intensive interest in the past two decades.[18−21] Upon rationale arrangement of donor and acceptor molecules, the light absorbed by the donor can be funneled to the acceptor and thus generate long-wave emission, which is very useful in energy conversion,[22,23] luminescence,[24] bioimaging,[25,26] and sensors.[27,28] However, energy transfer from the donor to acceptor becomes possible only as the dipole moments of the donor and the acceptor molecules orient appropriately or the distance between them is within 1−10 nm.[29] Because both the donor and acceptor are usually planar-conjugated molecules, they undergo $\pi-\pi$ stacking readily, which results in dramatic emission quenching. To avoid the undesired $\pi-\pi$ stacking, tremendous efforts have been input, such as tethering the donor and acceptor with a linker group in one molecule,[25,27,30,31] doping of acceptors in dendrimers,[32−34] or designing elegant molecular arrays of donor and acceptors using supramolecular self-assemblies.[35−40]

Herein, we report that upon employment of allosteric self-assembly, considerations about the arrangement of donor and acceptors in space are not necessary, and light-harvesting can be facilely generated in the arbitrary self-assembled donor−acceptor system. The underlying chemistry is that coordinating a metal ion to the head of a chromophore amphiphile TTC4L changes the dipole orientation of the terthiophene donor group tethering to the chain end (Scheme 1). This directly results in

Received: March 7, 2018
Revised: April 29, 2018
Published: April 30, 2018

DOI: 10.1021/acs.langmuir.8b00759
Langmuir 2018, 34, 5935−5942

Scheme 1. Illustration of Allosteric Self-Assembly-Facilitated Light Harvesting in the TTC4L−Metal Ion−4-(4-diethylaminostyryl)-1-methylpyridinium iodide (SMP) System[a]

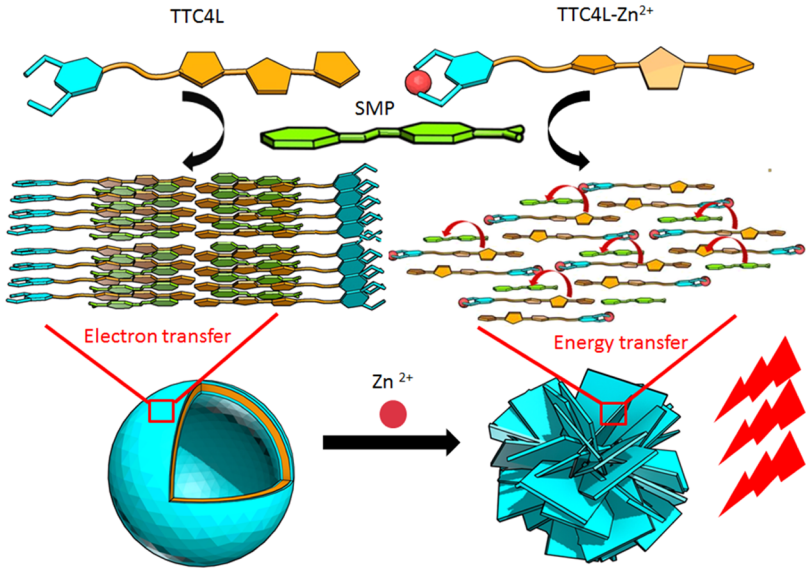

[a]Binding of metal ions to the coordinating head (blue) of TTC4L twists the terthiophene group (yellow) at the chain end, which changes the dipole orientation of the terthiophene (yellow). As a result, $\pi-\pi$ stacking of terthiophene and SMP is avoided, so that FRET occurs between them.

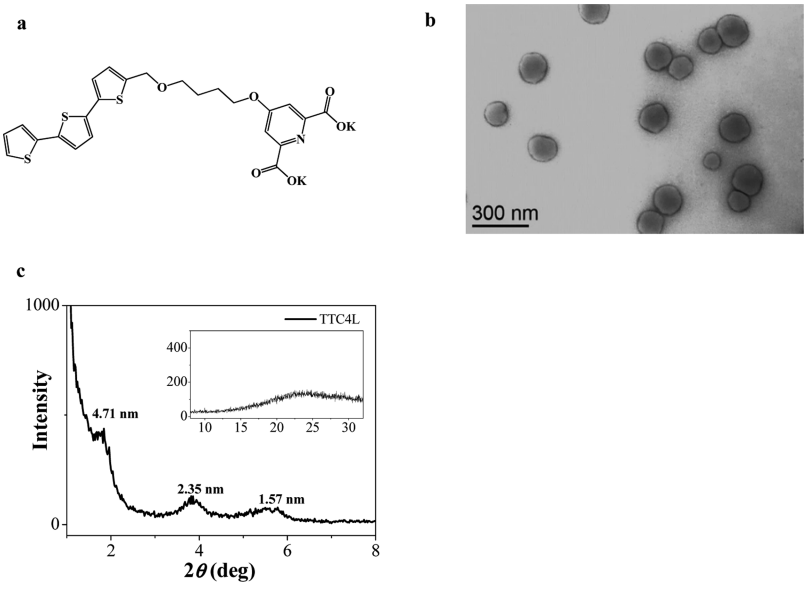

Figure 1. Self-assembly of TTC4L and TTC4L/Zn^{2+}. (a) Chemical structure of TTC4L. (b) TEM of TTC4L methanol solution (50 μM). (c) X-ray diffraction (XRD) result of TTC4L vesicles.

self-assembly of TT4CL transition from vesicles to flowerlike structures. As a result, FRET in the allosteric self-assembly becomes possible, whereas it is silenced in the vesicular self-assembly of TTC4L. Notice that the emission of the single donor group is not affected by binding of the metal ion at the remote head without self-assembly. FRET is facilitated by the transition of the self-assembly of TTC4L. This allosteric self-assembly allows facile regulation of both the structure and function of molecular self-assemblies via a postorganic synthesis strategy, which are expected to offer help in creating desired functional materials through a simple pathway.

RESULTS AND DISCUSSION

Zn^{2+}-Triggered Allosteric Self-Assembly of TTC4L. TTC4L is a coordinating amphiphile synthesized in our lab, which contains a fluorescent terthiophene group tethered to a coordinating head of pyridine dicarboxylate via an oxyl-butyl chain (Figure 1a).[41] The solubility of TTC4L in water is relatively small but can form a clear solution in methanol at concentrations below 200 μM. Transmission electron microscopy (TEM) observations reveal that TTC4L itself self-assembles into spherical vesicles (Figure 1b) with a well-defined cortex.[42] The average diameter of the vesicles is about 150 nm. Figure 1c shows that the TTC4L vesicles display typical lamellar diffractions. The distance of 4.71 nm is in good

DOI: 10.1021/acs.langmuir.8b00759
Langmuir 2018, 34, 5935−5942

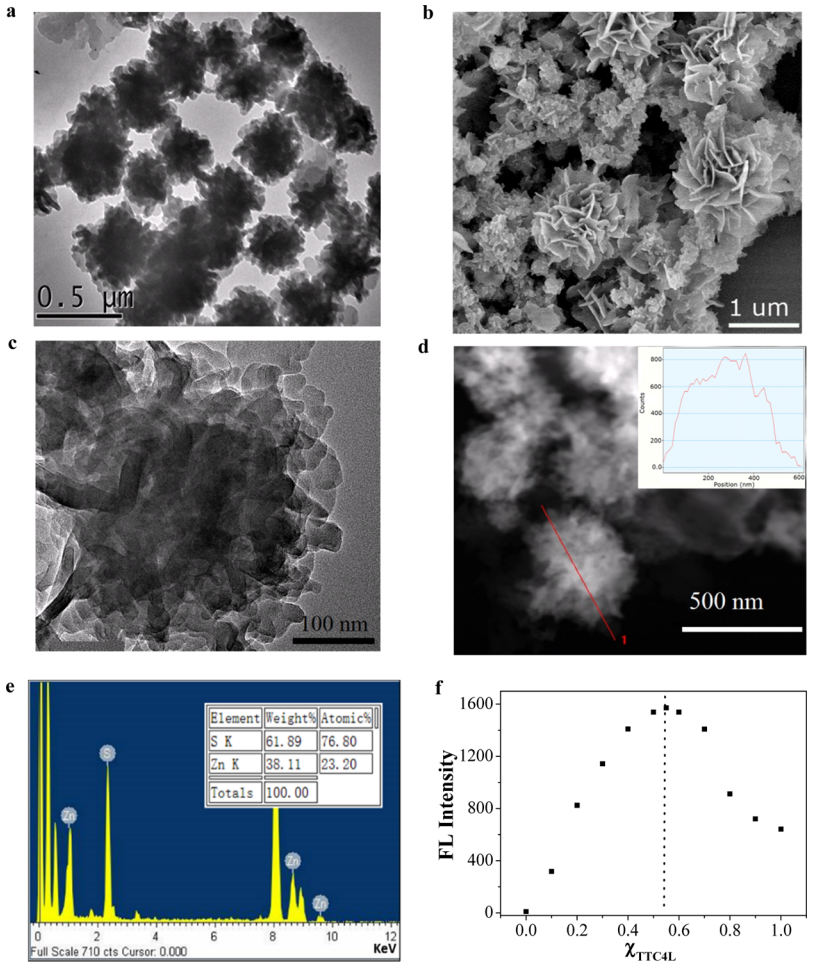

Figure 2. (a) TEM image of the freshly prepared TTC4L/Zn^{2+} (50−50 μM) in methanol. (b) Scanning electron microscopy (SEM) image of the TTC4L/Zn^{2+} self-assembly after aging 6 h. (c) Enlarged TEM image of the TTC4L/Zn^{2+} nanoflowers. (d) Scanning TEM image of the TTC4L/Zn^{2+} self-assembly showing the distribution of the Zn element. The content of Zn across the red line in (d) is given in the inset, which reveals that the Zn element is homogeneous throughout the self-assembly. (e) EDX data of TTC4L/Zn^{2+}. (f) Job's plot of TTC4L and Zn^{2+}. The total concentration of TTC4L and Zn^{2+} was kept constant at 100 μM. The measured fluorescence intensity was at the wavelength of 550 nm.

agreement with 2 times the extending length of TTC4L, confirming the presence of bilayers formed with TTC4L.

However, upon addition of $Zn(NO_3)_2$ at the molar ratio of TTC4L/$Zn(NO_3)_2$ = 1:1, the vesicles change into flowerlike structures with an average size of ∼400 nm (Figure 2a). On aging, the flowerlike nanoclusters can grow further into micro-nanometers (Figure 2b) and gradually settle down to the bottom of the test tube within 6 h but can be redispersed facilely upon shaking with hand, indicating that their density is larger than water. Enlarged TEM image (Figure 2c) shows that the flowerlike structures are formed by small nanoplates about 20 nm wide. Scanning mode of the TEM image (Figure 2d) reveals that the zinc element in the flowerlike structures is homogeneously distributed, indicating that the flowerlike structures have a solid interior. Fourier transform infrared (FT-IR) and X-ray photoelectron spectroscopy (XPS) measurements suggest that Zn^{2+} coordinates with the pyridine dicarboxylate headgroup of TTC4L (Figure S1) in the flowerlike structures. Variation of the molar ratio between TTC4L and $Zn(NO_3)_2$ does not change the morphology and size of the freshly prepared nanoclusters (Figure S2), indicating that the flowerlike nanoclusters have a fixed composition. Elemental analysis with energy-dispersive X-ray spectroscopy (EDX) (Figure 2e) reveals the presence of TTC4L and Zn^{2+} at a constant molar ratio of 1:1 in the flowers obtained at different TTC4L/$Zn(NO_3)_2$ systems (Figures 2e and S2). Meanwhile, a Job's plot obtained by measuring the fluorescence of TTC4L at varied TTC4L/Zn^{2+} molar ratios also suggests that the binding ratio is around 1:1 (Figure 2f). This means that TTC4L and Zn^{2+} form a charge-neutral TTC4L/Zn^{2+} coordination compound, which explains why variation of the molar ratio between TTC4L and $Zn(NO_3)_2$ does not affect the final self-assembled structure.

It is noteworthy that coordination of Zn^{2+} to the head of TTC4L did not change the electronic states of the terthiophene groups at the chain end. The UV−vis spectra in Figure 3a reveal that the absorption of the terthiophene group at 350 nm is not affected, only that for the pyridine dicarboxylate group at 250 nm blue shifts to 220 nm, indicating the subtraction of electrons from the dicarboxylate group because of the coordination with Zn^{2+}. Such a scenario was further confirmed by the fluorescence measurements. Figure 3b shows that for a very dilute solution of 10 μM, the emission spectra of TTC4L (Figure 3b, black line) and TTC4L/Zn^{2+} (Figure 3b, red line) are essentially the same. However, at the concentration of 50 μM where the nanoclusters are formed, the emission spectrum of TTC4L/Zn^{2+} is considerably different (Figure 3b, blue line). The occurrence of a broad emission at 550 nm was observed

DOI: 10.1021/acs.langmuir.8b00759
Langmuir 2018, 34, 5935−5942

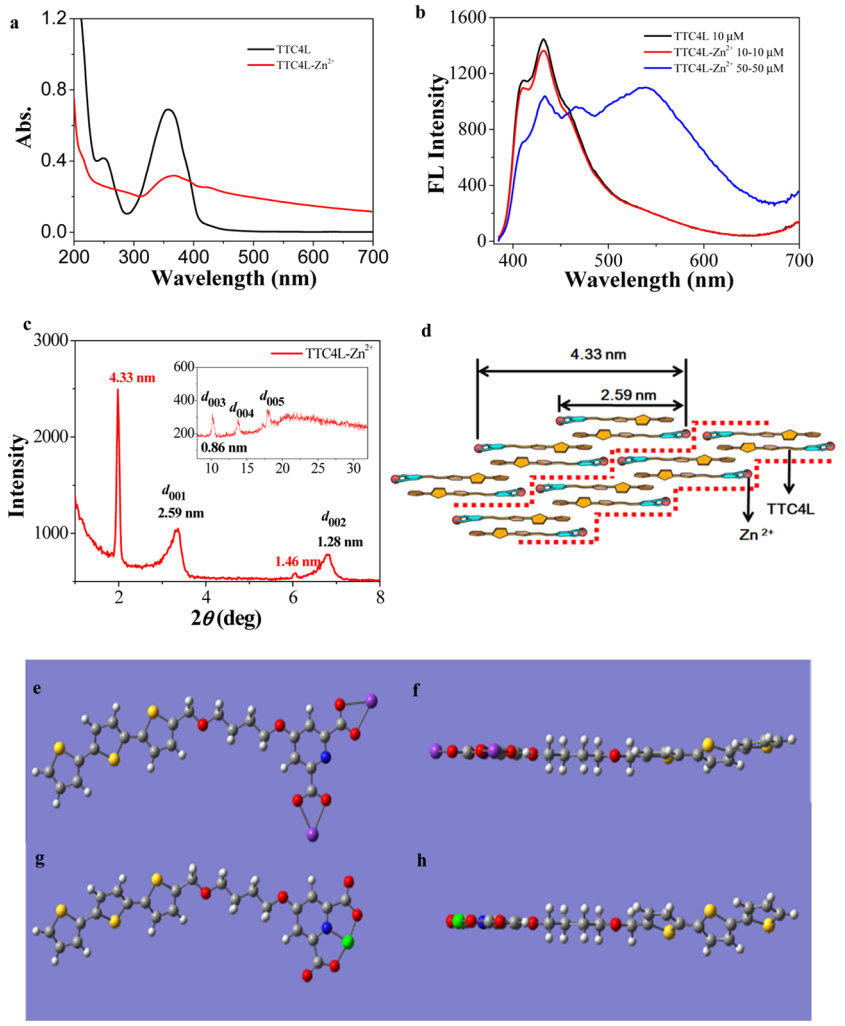

Figure 3. (a) Ultraviolet−visible (UV−vis) spectra of TTC4L and TTC4L/Zn^{2+}. (b) Fluorescence spectra of TTC4L/Zn^{2+} at nonaggregated (10 μM) and aggregated concentrations (50 μM). (c) XRD result of TTC4L/Zn^{2+}. (d) Scheme of the molecular arrangement in the nanoflowers. The dotted lines are eye-guiding lines for the arrangement of the complete interlaced bilayers of TTC4L/Zn^{2+}. (e−h) Molecular modulation of TTC4L and TTC4L/Zn^{2+}. (e,f) are the front view and side view of TTC4L (binding with $2K^{+}$). (g,h) are the front and side views of TTC4L/Zn^{2+}, respectively.

for the self-assembled TTC4L/Zn^{2+} system featuring the emission of excimers of the terthiophene moiety.[43−46] Lifetime measurements also confirm the presence of excimers, whereas it is absent in the TTC4L single system (Figure S3 and Table S1). This means that the coordination only changes the packing mode of TTC4L, which can be further verified by XRD measurements.

Different from the three broad diffraction peaks for the TTC4L vesicles in the low-angle region (Figure 1c), seven sharper diffraction peaks are obtained in the XRD measurement for the flowerlike clusters (Figure 3c). These peaks can be assigned to two groups of sublayers of a lamellar structure, one with distances of 4.33 nm (001) and 1.44 nm (003) and the other with distances of 2.59 nm (001), 1.28 nm (002), 0.86 nm (003), 0.64 nm (004), and 0.51 nm (005). The disappearance of the (002) diffraction in the first set of sublayers is probably caused by the distinction effect between the two sets of sublayers. Specifically, the distance attributed to the bilayers formed by the TTC4L molecules becomes smaller in the nanoflowers (4.33 nm) than in the vesicle (4.71 nm), suggesting that coordination has triggered the partially interlaced packing of the TTC4L molecules. It is noted that the distance of 2.59 nm for the 001 diffraction of the second set of layer is only slightly longer than the extending length of TTC4L (2.35 nm), and this layer is dominant throughout the structure so that the fifth diffraction is observed. This means that the TTC4L molecules in the coordinated system have arranged into completely interlaced bilayers upon coordination, as illustrated in Figure 3d. Obviously, the distance of 2.59 nm is from a pair of fully interlaced TTC4L/Zn^{2+} supramolecules, whereas the distance of 4.33 nm is from the partial interlaced pair of TTC4L/Zn^{2+}.

We expect that the change of packing mode of TTC4L in the TTC4L/Zn^{2+} nanoflowers originates from the coordination triggered chain twisting of TTC4L. To verify this argument, quantum chemistry calculation was adopted to reveal the conformation of the TTC4L molecules upon coordination with Zn^{2+}. The results are listed in Figure 3e−h. It clearly shows that the terthiophene groups are arranged in an almost planar mode before coordination (Figure 3e,f), whereas coordination with Zn^{2+} triggers considerable twisting of the terthiophene plane at the chain end (Figure 3g,h). As a result, $\pi-\pi$ stacking between the terthiophene groups becomes difficult, and the molecules have to form interlaced pairs to minimize energy. However,

DOI: 10.1021/acs.langmuir.8b00759
Langmuir 2018, 34, 5935−5942

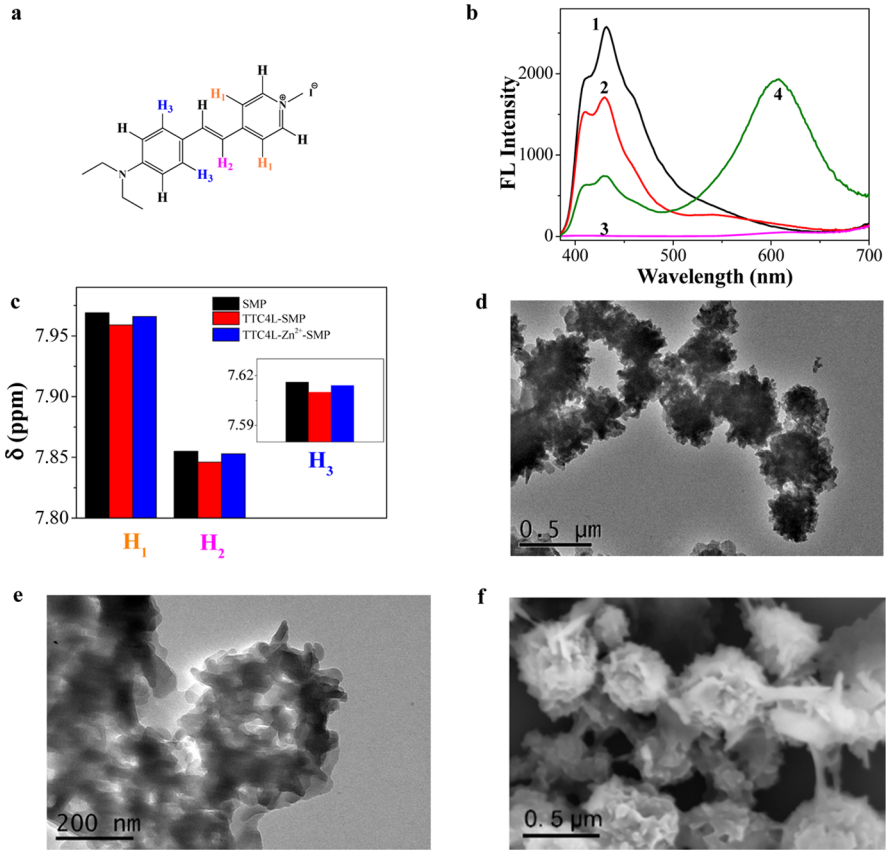

Figure 4. Evoked light harvesting of TTC4L and SMP triggered by allosteric effector Zn^{2+}. (a) Chemical structure of SMP. (b) Fluorescence spectra of TTC4L-containing system. (c) ^1H NMR chemical shift of SMP in the light-harvesting system. (d,e) TEM result of TTC4L/Zn^{2+}/SMP. (f) SEM image of the TTC4L/Zn^{2+}/SMP nanoclusters.

$\pi-\pi$ stacking between the last thiophene ring of interlaced pairs is still possible, which generates excimers.

Allosteric Self-Assembly-Enabled Light Harvesting. Thiophenes are well-known organic dyes rich in electrons, which have great potential in optoelectronics, photocatalysis, sensors, and luminescence. With the terthiophene moiety imbedded in the molecule, TTC4L can serve as an energy donor when paired with a cationic fluorescent dye SMP (Figure 4a) because the emission of TTC4L overlaps well with the absorption of SMP (Figure S4). However, obvious fluorescence quenching of TTC4L occurs immediately when the two are mixed in methanol (Figure 4b, line 2), and a decrease of the lifetime of TTC4L is observed (Figure S3a and Table S1). Variation of the molar ratio between TTC4L and SMP only changes the degree of fluorescence quenching (Figure S5). In the meanwhile, no emission of SMP is observed. ^1H nuclear magnetic resonance (NMR) measurements suggest that the chemical shifts of SMP have shifted to upper field (Figures 4c and S6), indicating the occurrence of $\pi-\pi$ interaction between SMP and the terthiophene group. TEM and dynamic light scattering measurements reveal that addition of SMP to the vesicular system of TTC4L does not change the size and morphology of the vesicles noticeably (Figure S7).

However, upon addition of $Zn(NO_3)_2$ to the TTC4L/SMP system, the red fluorescence of SMP is observed immediately (Figure 4b, line4) along with the increase of lifetime of SMP (Figure S4b and Table S2), signifying the occurrence of FRET. TEM and SEM observations reveal that the vesicles change into the same flowerlike nanoclusters observed in the TTC4L/Zn^{2+} system (Figure 4d–f), indicating that the structural transition is solely triggered by the binding of Zn^{2+} to the head of TTC4L. XRD pattern reveals that the sublayers of TTC4L/Zn^{2+} are still there, although the peak intensity varies (Figure S8). But a peak featuring the 2 times extended length of SMP, 1.95 nm, occurs at $2\theta = 4.5°$ in the XRD measurement (Figure S8). This means that the SMP molecules have inserted into the bilayers of TTC4L/Zn^{2+}. The possible location of SMP in the TTC4L/Zn^{2+} bilayer is the eye-guiding lines in Figure 3d, as illustrated in Scheme 1. Notice that the ^1H NMR measurements reveal that the chemical shifts of SMP in the clusters are almost the same as those in the SMP single solution (Figures 4c and S6). This is in clear contrast to the distinct chemical shifts of SMP in the TTC4L/SMP dual system, suggesting that Zn^{2+} has triggered a weaker interaction between the donor and acceptor, which enables the occurrence of FRET. Because the 1:1 binding of Zn^{2+} to the coordinating head does not change the hydrophilic and hydrophobic portion of TTC4L drastically, we attribute the drastic change in molecular packing to the conformational change, especially to the twisting of the terthiophene group. The dipole orientation of the twister terthiophene plane differs significantly from that of the planar SMP, so that no specific interactions occur between them, which finally lead to efficient energy transfer from TTC4L and SMP.

Generality of Allosteric Assembly-Triggered Light Harvesting. The metal ion-triggered allosteric effect is a general phenomenon. Besides $Zn(NO_3)_2$, other metal nitrates, such as $Cd(NO_3)_2$ and $Al(NO_3)_3$, can also drive allosteric self-

DOI: 10.1021/acs.langmuir.8b00759
Langmuir 2018, 34, 5935−5942

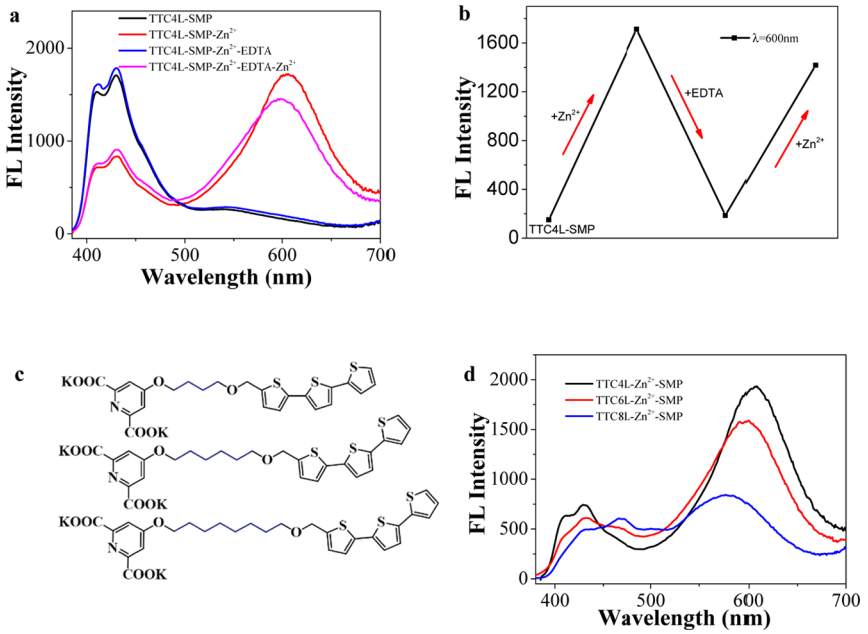

Figure 5. "On–off" and distance-dependent light-harvesting behavior in the allosteric self-assembly system. (a) Fluorescence spectra of the TTC4L/SMP FRET system affected by Zn^{2+} and EDTA. (b) Fluorescence intensity at 600 nm of the TTC4L/SMP FRET system affected by Zn^{2+} and EDTA. (c) Chemical structures of TTC*n*L (n = 4, 6, 8). (d) Fluorescence spectra of the TTC*n*L/Zn^{2+}/SMP light-harvesting system.

assembly and awaken light harvesting between TTC4L and SMP (Figure S9), but the efficiency of light harvesting differs from metal to metal because of different triggered conformations. However, in all cases, the allosteric self-assembly-enabled light harvesting can be produced either by addition of metal ions to the mixture of TTC4L/SMP or by addition of SMP to the TTC4L–metal ion coordinating system. Figure S10 shows that no changes were observed in both the emission spectra (Figure S10a) and the TEM image (Figure S10b). EDX (Figure S11) measurement suggests that the molar ratio of TTC4L/Zn^{2+} is 1:1 even in the presence of SMP, indicating that the conformational change triggered by coordination is crucial for the occurrence of FRET. Furthermore, no FRET occurs at dilute TTC4L/Zn^{2+} solution where no self-assembly occurs, suggesting that the FRET is mediated by the allosteric self-assembly. Because metal ions can be removed by addition of a competitive ligand, the FRET can be switched on and off. Figure 5a shows that upon removal of Zn^{2+} with ethylenediaminetetraacetic acid (EDTA), the FRET phenomenon vanishes, whereas it occurs again by feeding Zn^{2+} to the system. This process is repeatable (Figure 5b), which reveals a typical "on–off" behavior.

Chain Length Dependence of the Light-Harvesting Efficiency in the Allosteric Self-Assembly. Furthermore, the allosteric effect has a strong distance effect. In the DNA allosteric system, effective allosteric effect was found within several base pairs.[9] Similarly, we found that the light-harvesting efficiency is closely related to the length of the linker chain between the terthiophene group and the coordinating head. As the chain length increases from 4 to 6 (TTC6L) and 8 (TTC8L) carbons (Figure 5c), the FRET efficiency decreases significantly (Figure 5d). Quantum chemistry calculation results infer that the longer the linker chain is, the smaller is the extent of twisting of terthiophene that can be induced (Figure S12). Our results strongly indicate that upon employment of allosteric self-assembly, we are able to control both the structure and function of self-assembled materials.

CONCLUSIONS

In summary, allosteric self-assembly can be used to control the self-assembled structure and its function. We show that upon binding the metal ion at the headgroup, the conformational change of the amphiphile TTC4L may lead to change of the dipole orientation of the energy donor at the chain end. This on the one hand leads to a drastically different self-assembled structure; on the other hand, it enables light harvesting between the donor–acceptor based on FRET. In analogy with the allosteric effect in biological systems, the distance between the functional site and the binding site is also very relevant to the efficiency of light harvesting. The longer the linker is, the weaker is the allosteric effect. Because the FRET efficiency is gated by metal ions, controlling the feeding of metal ions allows switching on and off of light harvesting. We expect that using allosteric self-assembly, we will be able to create abundant structures with distinct function from limited molecules. In this regard, allosteric self-assembly is expected to show prominent potential for the postorganic synthesis control over the structure and function of self-assembled materials.

EXPERIMENTAL SECTION

Materials. TTC4L was synthesized according to the procedures reported in our previous work.[41] TTC6L and TTC8L were synthesized in this work (Scheme S1); the synthetic method was similar to TTC4L. SMP was purchased from Sigma-Aldrich Co. and used without further purification. $Zn(NO_3)_2$ was purchased from Beijing Chemical Reagents Co. (AR grade). EDTA disodium salt dihydrate, 99%, was purchased from J&K Chemicals. Solvent methanol was purchased from Beijing Chemical Reagents Co. (AR grade). The desired amounts of TTC4L, $Zn(NO_3)_2$, and SMP were added into the methanol solvent sequentially. In a typical procedure, TTC4L, $Zn(NO_3)_2$, and SMP were mixed in the molar ratio of 1:1:1 with a total concentration of 150 μM, unless stated otherwise. All solutions were prepared fresh and kept away from light. All experiments were performed at room temperature (~25 °C), unless stated otherwise.

TEM Observations. TTC4L TEM images were recorded on a JEM-100CX II transmission electron microscope (JEOL, Japan, 80

DOI: 10.1021/acs.langmuir.8b00759
Langmuir 2018, 34, 5935–5942

kV). The other self-assembled structures were characterized by TEM (FEI Tecnai G2 T20, 120 kV, together with energy-dispersive spectroscopy measurement). The samples were prepared by dropping solutions onto copper grids coated with the Formvar film. Excess water was removed by a filter paper, and the samples were dried in an ambient environment at room temperature for TEM observation. In case of the TTC4L or TTC4L/SMP samples, they were negatively stained by uranyl acetate before water removal. The samples containing Zn^{2+} were observed directly without staining.

Fluorescence Measurements. Fluorescence spectra were obtained with a Hitachi F-7000 fluorescence spectrometer. The excitation wavelength was 365 nm. The slit for excitation and emission was 5 nm. The scanning rate was 1200 nm min^{-1}. The scanning voltage of the Xe lamp was set at 700 V.

Fluorescence Life Measurements. The fluorescence lifetime measurement was performed on a FLS980 spectrometer (Edinburgh Instrument) with a 355 nm laser source. The lifetime curves were fitted with the two-exponential decay eq 1 and three-exponential decay eq 2.

$$I_t = I_1 e^{-t/\tau_1} + I_2 e^{-t/\tau_2} \quad (1)$$

$$I_t = I_1 e^{-t/\tau_1} + I_2 e^{-t/\tau_2} + I_3 e^{-t/\tau_3} \quad (2)$$

where I_t is the change in absorbance at time t and τ is the lifetime.

UV−Vis Measurements. UV−vis spectra were obtained with a spectrometer (Shimadzu, UV-1800) using a 10 mm quartz cell in the range of 200−700 nm with a step size of 0.5 nm.

^{1}H NMR Measurements. ^{1}H NMR spectra were acquired on Bruker AVANCE III 500 MHz NMR spectrometer with 512 scanning times. The samples were prepared in methanol-d_4.

FT-IR Measurements. FT-IR spectra were measured with a spectrometer (Thermo Scientific, Nicolet iN10 MX). Drops of samples were put onto a diamond window plate and dried under ambient conditions. The spectra were collected from 4000 to 600 cm^{-1} with 16 scanning times with the transmission mode.

XPS. XPS measurements were performed with an X-ray photoelectron spectrometer (Kratos Analytical Ltd., AXIS ULTRA). Several drops of samples were put onto a silicon wafer and allowed to dry under ambient conditions. With Al Kα ($h\nu$ = 1486.7 eV) as the X-ray source, the operating voltage is 15 kV and the emission current is 40 mA.

XRD Measurements. XRD results were performed with an X-ray diffractometer (Rigaku D/MAX-2000, Ni-filtered Cu Kα radiation); the operating voltage is 40 kV and the emission current is 100 mA. The DivSlit, SctSlit, and RecSlit were 1/6, 1/6 and 0.15 nm, respectively, when the measured range is from 0.6 to 8°, and the DivSlit, SctSlit and RecSlit were 1/2, 1/2 and 0.30 nm, respectively, when the measured range is from 3 to 30°.

Quantum Chemistry Calculation. Molecule modeling was calculated at the restricted density functional theory level. The hybrid functional B3LYP and the 6-311+g(d,p) basis set were used. All calculations were performed using the Gaussian 09 package.

■ ASSOCIATED CONTENT

Supporting Information

The Supporting Information is available free of charge on the ACS Publications website at DOI: 10.1021/acs.langmuir.8b00759.

Synthesis of TTC6L and TTC8L, Tables S1 and S2, and Figures S1−S12 (PDF)

■ AUTHOR INFORMATION

Corresponding Authors

*E-mail: xiaoyl@pku.edu.cn (Y.X.).

*E-mail: yunyan@pku.edu.cn (Y.Y.).

ORCID

Yun Yan: 0000-0001-8759-3918

Notes

The authors declare no competing financial interest.

■ ACKNOWLEDGMENTS

This work is supported by the National Science Foundation of China (NSFC, grant no. 21573011) and the National Basic Research Program of China (2013CB933800). We thank Dr. Lingxiang Jiang for fruitful discussion.

■ REFERENCES

(1) Forman, B. M.; Umesono, K.; Chen, J.; Evans, R. M. Unique Response Pathways Are Established by Allosteric Interactions Among Nuclear Hormone Receptors. *Cell* **1995**, *81*, 541−550.

(2) Xiao, T.; Takagi, J.; Coller, B. S.; Wang, J.-H.; Springer, T. A. Structural Basis for Allostery in Integrins and Binding to Fibrinogen-MimeticTherapeutics. *Nature* **2004**, *432*, 59−67.

(3) Gunasekaran, K.; Ma, B.; Nussinov, R. Is Allostery an Intrinsic Property of All Dynamic Proteins? *Proteins* **2004**, *57*, 433−443.

(4) Fenton, A. W. Allostery: an Illustrated Definition for the "Second Secret of Life". *Trends Biochem. Sci.* **2008**, *33*, 420−425.

(5) Guo, J.; Zhou, H.-X. Protein Allostery and Conformational Dynamics. *Chem. Rev.* **2016**, *116*, 6503−6515.

(6) Nussinov, R.; Tsai, C.-J. Allostery in Disease and in Drug Discovery. *Cell* **2013**, *153*, 293−305.

(7) Law, A. B.; Sapienza, P. J.; Zhang, J.; Zuo, X.; Petit, C. M. Native State Volume Fluctuations in Proteins as a Mechanism for Dynamic Allostery. *J. Am. Chem. Soc.* **2017**, *139*, 3599−3602.

(8) Chaires, J. B. Allostery: DNA Does It, Too. *ACS Chem. Biol.* **2008**, *3*, 207−209.

(9) Kim, S.; Brostromer, E.; Xing, D.; Jin, J.; Chong, S.; Ge, H.; Wang, S.; Gu, C.; Yang, L.; Gao, Y. Q.; Su, X.-d.; Sun, Y.; Xie, X. S. Probing Allostery Through DNA. *Science* **2013**, *339*, 816−819.

(10) Porchetta, A.; Idili, A.; Vallée-Bélisle, A.; Ricci, F. General Strategy to Introduce pH-Induced Allostery in DNA-Based Receptors to Achieve Controlled Release of Ligands. *Nano Lett.* **2015**, *15*, 4467−4471.

(11) Changeux, J.-P. The Origins of Allostery: From Personal Memories to Material for the Future. *J. Mol. Biol.* **2013**, *425*, 1396−1406.

(12) Strickland, D.; Moffat, K.; Sosnick, T. R. Light-Activated DNA Binding in a Designed Allosteric Protein. *Proc. Natl. Acad. Sci. U.S.A.* **2008**, *105*, 10709−10714.

(13) Choi, J. H.; Laurent, A. H.; Hilser, V. J.; Ostermeier, M. Design of Protein Switches Based on an Ensemble Model of Allostery. *Nat. Commun.* **2015**, *6*, 6968.

(14) Lifschitz, A. M.; Rosen, M. S.; McGuirk, C. M.; Mirkin, C. A. Allosteric Supramolecular Coordination Constructs. *J. Am. Chem. Soc.* **2015**, *137*, 7252−7261.

(15) Ulrich, S.; Petitjean, A.; Lehn, J.-M. Metallo-Controlled Dynamic Molecular Tweezers: Design, Synthesis, and Self-Assembly by Metal-Ion Coordination. *Eur. J. Inorg. Chem.* **2010**, 1913−1928.

(16) Marlin, D. S.; Cabrera, D. G.; Leigh, D. A.; Slawin, A. M. Z. An Allosterically Regulated Molecular Shuttle. *Angew. Chem., Int. Ed.* **2006**, *45*, 1385−1390.

(17) Kremer, C.; Lützen, A. Artificial Allosteric Receptors. *Chem.—Eur. J.* **2013**, *19*, 6162−6196.

(18) Basham, J. I.; Mor, G. K.; Grimes, C. A. Forster Resonance Energy Transfer in Dye-Sensitized Solar Cells. *ACS Nano* **2010**, *4*, 1253−1258.

(19) Frischmann, P. D.; Mahata, K.; Würthner, F. Powering the Future of Molecular Artificial Photosynthesis with Light-Harvesting Metallosupramolecular Dye Assemblies. *Chem. Soc. Rev.* **2013**, *42*, 1847−1870.

(20) Ajayaghosh, A.; Praveen, V. K.; Vijayakumar, C. Organogels as Scaffolds for Excitation Energy Transfer and Light Harvesting. *Chem. Soc. Rev.* **2008**, *37*, 109−122.

DOI: 10.1021/acs.langmuir.8b00759
Langmuir 2018, 34, 5935−5942

(21) Yuan, L.; Lin, W.; Zheng, K.; Zhu, S. FRET-Based Small-Molecule Fluorescent Probes: Rational Design and Bioimaging Applications. *Acc. Chem. Res.* **2013**, *46*, 1462−1473.
(22) Frischmann, P. D.; Mahata, K.; Würthner, F. Powering the Future of Molecular Artificial Photosynthesis with Light-Harvesting Metallosupramolecular Dye Assemblies. *Chem. Soc. Rev.* **2013**, *42*, 1847−1870.
(23) Rao, K. V.; Datta, K. K. R.; Eswaramoorthy, M.; George, S. J. Light-Harvesting Hybrid Assemblies. *Chem.—Eur. J.* **2012**, *18*, 2184−2194.
(24) Serin, J. M.; Brousmiche, D. W.; Fréchet, J. M. J. A FRET-Based Ultraviolet to Near-Infrared Frequency Converter. *J. Am. Chem. Soc.* **2002**, *124*, 11848−11849.
(25) Aron, A. T.; Loehr, M. O.; Bogena, J.; Chang, C. J. An Endoperoxide Reactivity-Based FRET Probe for Ratiometric Fluorescence Imaging of Labile Iron Pools in Living Cells. *J. Am. Chem. Soc.* **2016**, *138*, 14338−14346.
(26) Jia, X.; Chen, Q.; Yang, Y.; Tang, Y.; Wang, R.; Xu, Y.; Zhu, W.; Qian, X. FRET-Based Mito-Specific Fluorescent Probe for Ratiometric Detection and Imaging of Endogenous Peroxynitrite: Dyad of Cy3 and Cy5. *J. Am. Chem. Soc.* **2016**, *138*, 10778−10781.
(27) Miyawaki, A. Exploiting the Cyanobacterial Light-Harvesting Machinery for Developing Fluorescent Probes. *Nat. Methods* **2016**, *13*, 729−730.
(28) Scholler, P.; Moreno-Delgado, D.; Lecat-Guillet, N.; Doumazane, E.; Monnier, C.; Charrier-Savournin, F.; Fabre, L.; Chouvet, C.; Soldevila, S.; Lamarque, L.; Donsimoni, G.; Roux, T.; Zwier, J. M.; Trinquet, E.; Rondard, P.; Pin, J.-P. HTS-compatible FRET-Based Conformational Sensors Clarify Membrane Receptor Activation. *Nat. Chem. Biol.* **2017**, *13*, 372−380.
(29) Sahoo, H. Foerster resonance energy transfer - A Spectroscopic Nanoruler: Principle and Applications. *J. Photochem. Photobiol., C* **2011**, *12*, 20−30.
(30) Jadhav, P. D.; Shen, J.; Sammynaiken, R.; Reaney, M. J. T. Site Covalent Modification of Methionyl Peptides for Production of FRET Complexes. *Chem.—Eur. J.* **2015**, *21*, 17023−17034.
(31) Kaur, A.; Haghighatbin, M. A.; Hogan, C. F.; New, E. J. A FRET-Based Ratiometric Redox Probe for Detecting Oxidative Stress by Confocal Microscopy, FLIM and flow cytometry. *Chem. Commun.* **2015**, *51*, 10510−10513.
(32) Schenning, A. P. H. J.; Peeters, E.; Meijer, E. W. Energy Transfer in Supramolecular Assemblies of Oligo(p-phenylene vinylene)s Terminated Poly(propylene imine) Dendrimers. *J. Am. Chem. Soc.* **2000**, *122*, 4489−4495.
(33) Hahn, U.; Gorka, M.; Vögtle, F.; Vicinelli, V.; Ceroni, P.; Maestri, M.; Balzani, V. Light-Harvesting Dendrimers: Efficient Intra- and Intermolecular Energy-Transfer Processes in a Species Containing 65 Chromophoric Groups of Four Different Types. *Angew. Chem., Int. Ed.* **2002**, *41*, 3595−3598.
(34) Zeng, Y.; Li, Y.; Li, M.; Yang, G.; Li, Y. Enhancement of Energy Utilization in Light-Harvesting Dendrimers by the Pseudorotaxane Formation at Periphery. *J. Am. Chem. Soc.* **2009**, *131*, 9100−9106.
(35) Ajayaghosh, A.; Vijayakumar, C.; Praveen, V. K.; Babu, S. S.; Varghese, R. Self-Location of Acceptors as "Isolated" or "Stacked" Energy Traps in a Supramolecular Donor Self-Assembly: A Strategy to Wavelength Tunable FRET Emission. *J. Am. Chem. Soc.* **2006**, *128*, 7174−7175.
(36) Zhang, X.; Chen, Z.-K.; Loh, K. P. Coordination-Assisted Assembly of 1-D Nanostructured Light-Harvesting Antenna. *J. Am. Chem. Soc.* **2009**, *131*, 7210−7211.
(37) Kumar, C. V.; Duff, M. R. DNA-Based Supramolecular Artificial Light Harvesting Complexes. *J. Am. Chem. Soc.* **2009**, *131*, 16024−16026.
(38) Pu, F.; Wu, L.; Ran, X.; Ren, J.; Qu, X. G-Quartet-Based Nanostructure for Mimicking Light-Harvesting Antenna. *Angew. Chem., Int. Ed.* **2015**, *54*, 892−896.
(39) Bösch, C. D.; Langenegger, S. M.; Häner, R. Light-Harvesting Nanotubes Formed by Supramolecular Assembly of Aromatic Oligophosphates. *Angew. Chem., Int. Ed.* **2016**, *55*, 9961−9964.
(40) Zhang, D.; Liu, Y.; Fan, Y.; Yu, C.; Zheng, Y.; Jin, H.; Fu, L.; Zhou, Y.; Yan, D. Hierarchical Self-Assembly of a Dandelion-Like Supramolecular Polymer into Nanotubes for use as Highly Efficient Aqueous Light-Harvesting Systems. *Adv. Funct. Mater.* **2016**, *26*, 7652−7661.
(41) Zhao, L.; Cheng, X.; Ding, Y.; Yan, Y.; Huang, J. A Surfactant-Assisted Unimolecular Platform for Multicolor Emissions. *Soft Matter* **2012**, *8*, 10472−10478.
(42) Watson, M. L. Staining of Tissue Sections for Electron Microscopy with Heavy Metals. *J. Cell Biol.* **1958**, *4*, 475−478.
(43) Fujitsuka, M.; Cho, D. W.; Ohshita, J.; Kunai, A.; Majima, T. Fluorescence Properties of Si-Linked Oligothiophenes. *J. Phys. Chem. C* **2007**, *111*, 1993−1998.
(44) Tsai, W.-W.; Li, L.-s.; Cui, H.; Jiang, H.; Stupp, S. I. Self-Assembly of Amphiphiles with Terthiophene and Tripeptide Segments into Helical Nanostructures. *Tetrahedron* **2008**, *64*, 8504−8514.
(45) Mróz, W.; Bombenger, J.; Botta, C.; Biroli, A. O.; Pizzotti, M.; De Angelis, F.; Belpassi, L.; Tubino, R.; Meinardi, F. Oligothiophenes Nano-organized on a Cyclotetrasiloxane Scaffold as a Model of a Silica-Bound Monolayer: Evidence for Intramolecular Excimer Formation. *Chem.—Eur. J.* **2009**, *15*, 12791−12798.
(46) Deepak, V. D.; Sundararajan, P. R. Solvent Mixture Induced Self Assembly of a Terthiophene Based Rod-Coil Block Co-oligomer. *J. Phys. Chem. B* **2011**, *115*, 8458−8464.

DOI: 10.1021/acs.langmuir.8b00759
Langmuir 2018, 34, 5935−5942